

## Supporting Information

# *Improved activity for the oxygen evolution reaction using a tiara-like thiolate-protected nickel nanocluster*

Sota Funaki,<sup>a</sup> Tokuhisa Kawawaki,<sup>a,b,\*</sup> Tomoshige Okada,<sup>a</sup> Kana Takemae,<sup>a</sup> Sakiat Hossain,<sup>b</sup> Yoshiki Niihori,<sup>b</sup> Takumi Naito,<sup>c</sup> Makito Takagi,<sup>c</sup> Tomomi Shimazaki,<sup>c</sup> Soichi Kikkawa,<sup>d</sup> Seiji Yamazoe,<sup>d</sup> Masanori Tachikawa,<sup>c</sup> and Yuichi Negishi<sup>a,b,\*</sup>

<sup>a</sup>Department of Applied Chemistry, Faculty of Science, Tokyo University of Science, 1-3 Kagurazaka, Shinjuku-ku, Tokyo 162-8601, Japan

<sup>b</sup>Research Institute for Science and Technology, Tokyo University of Science, 1-3 Kagurazaka, Shinjuku-ku, Tokyo 162-8601, Japan

<sup>c</sup>Graduate School of NanoBioScience, Yokohama City University, 22-2 Seto, Kanazawa-ku, Yokohama 236-0027, Japan

<sup>d</sup>Department of Chemistry, Graduate School of Science, Tokyo Metropolitan University, 1-1 Minami-Osawa, Hachioji-shi, Tokyo 192-0397, Japan

\*Corresponding author E-mail: kawawaki@rs.tus.ac.jp (T.K.), negishi@rs.tus.ac.jp (Y.N.)

## 1 Chemicals

All chemicals were commercially obtained and used without further purification. Nickel nitrate hydroxide [Ni(NO<sub>3</sub>)<sub>2</sub>·6H<sub>2</sub>O], Iridium tetrachloride [Ir(Cl)<sub>4</sub>], potassium hydroxide (KOH), triethylamine (NEt<sub>3</sub>), Ni standard solution (1000 mg L<sup>-1</sup>), yttrium standard solution (1000 ppm), Nafion dispersion solution, and pure water were obtained from FUJIFILM Wako Pure Chemical Co (Japan). Acetone, *n*-propanol, 2-propanol, methanol (MeOH), hexane, tetrahydrofuran (THF), dichloromethane (DCM), hydrochloric acid, and nitric acid were obtained from Kanto Chemical Co., Inc (Japan). The 2-phenylethanethiol was obtained from Sigma Aldrich (USA). *trans*-2-[3-(4-*tert*-Butylphenyl)-2-methyl-2-propenylidene]malononitrile (DCTB) was obtained from Tokyo Kasei (Japan). Carbon black (CB; Vulcan XC-72), dried under vacuum before use, was obtained from Fuel Cell Earth Co., Inc (Japan).

## 2. Characterization

Matrix-assisted laser desorption/ionization (MALDI) mass spectra were recorded with a JMS-S3000 spiral time-of-flight mass spectrometer (JEOL, Tokyo, Japan) equipped with a semiconductor laser ( $\lambda = 349$  nm). DCTB was used as the MALDI matrix. To minimize nanocluster (NC) dissociation induced by laser irradiation, the sample-to-matrix ratio was fixed at 1:1000.

Ultraviolet-visible (UV-vis) absorption spectra of products were acquired in dichloromethane at 25 °C with a V-630 spectrometer (JASCO, Tokyo, Japan).

Fourier-transform infrared (FT-IR) spectra of the products were obtained using the attenuated total reflectance (ATR) method in the region between 400 and 4000 cm<sup>-1</sup> with a FT/IR-4600-ATR-PRO ONE spectrometer (JASCO, Tokyo, Japan) equipped with a DLATGS detector as the average of 50 scans at 4-cm<sup>-1</sup> resolution.

Inductively coupled plasma-mass spectrometry was performed with an Agilent 7850 spectrometer (Agilent Technologies, Tokyo, Japan). Yttrium was used as the internal standard.

Ni K-edge X-ray absorption fine structure (XAFS) measurements were performed at beamline BL01B1 of the SPring-8 facility of the Japan Synchrotron Radiation Research Institute (proposal numbers 2020A0695, 2021A1102, 2021B1163, 2022A1075 and 2022B1823). The incident X-ray beam was monochromatized with a Si(111) double-crystal monochromator. As references, XAFS spectra of Ni foil, solid NiO, and solid Ni(OH)<sub>2</sub> were recorded in transmission mode with ionization chambers. The Ni K-edge XAFS spectra of the samples were measured in fluorescence mode with a 19-element Ge solid-state detector at room temperature. The X-ray energies for the Ni K-edges were calibrated with Ni foil. The X-ray absorption near-edge structure (XANES) and extended XAFS (EXAFS) spectra were analyzed with xTunes<sup>1</sup> as follows. The  $\chi$  spectra were extracted by subtracting the atomic absorption background using cubic spline interpolation and normalized to the edge height.

The normalized data were used as the XANES spectra. The  $k^3$ -weighted  $\chi$  spectra in the  $k$  range 3.0–14.0 Å<sup>-1</sup> for the Ni K-edge were Fourier-transformed into  $r$  space for structural analysis.

Transmission electron microscope (TEM) images were obtained with a H-9500 electron microscope (HITACHI, Tokyo, Japan) or a JEM-2100 electron microscope (JEOL, Tokyo, Japan) operating at 200 kV, typically using a magnification of 600,000.

Powder X-ray diffraction (PXRD) patterns of the samples were measured with a Rint2500 diffractometer (Rigaku) with a Cu-K $\alpha$  source operated at 40 kV and 200 mA. A reflection-free silicon plate was used as a substrate.

All calculations were performed with the Gaussian 16 package<sup>2</sup>. The ground-state structures were optimized by density functional theory (DFT) with B3LYP using the LanL2DZ basis set for the Ni atoms and the 6-31G(d) basis set for the other atoms. Based on the optimized ground-state structure, absorption spectra were calculated using the time-dependent density functional theory (TD-DFT). For calculations considering solvation effects, the Polarizable Continuum Model (PCM) using the integral equation formalism (IEFPCM) was used.

Inductively coupled plasma mass spectrometry (ICP-MS) was performed with an Agilent 7500c spectrometer (Agilent Technologies, Tokyo, Japan). Yttrium was used as the internal standard.

### 3. Crystal data

#### 3.1 Data deposition information

Deposition numbers CCDC 2212626 (for **2** at 100.15 K) contain the supplementary crystallographic data for this paper. These data are provided free of charge by the joint Cambridge Crystallographic Data Centre and Fachinformationszentrum (FIZ) Karlsruhe. It can be accessed with the following link: <https://www.ccdc.cam.ac.uk/structures/>.

#### 3.2 Experiments and software used for obtaining geometric structures

A single crystal was immersed in cryoprotectant Parabar 10312 (Hampton Research, 34 Journey, Aliso Viejo, CA 92656-3317 USA) and mounted onto a MicroCrystal Mounts Assortment (MiTeGen, LLC, Ithaca, NY, USA). The X-ray diffraction data sets were collected with a Bruker D8 QUEST, with monochromated MoK $\alpha$  radiation ( $\lambda = 0.71073$  Å). The geometric structure of **2** was solved with Shelxt<sup>3</sup> (using the intrinsic phasing method) in Bruker Apex 4<sup>4</sup> suite GUI. Because the diffraction data quality was good, all of the atoms were solved in the first attempt. Subsequently, they were refined using the full-matrix least-squares method against F2 with SHELXL-2018/3 in Olex2 GUI.<sup>5-6</sup> DCM was highly disordered, which was resolved by dividing the occupancy of the carbon atom of the DCM. Finally, H atoms were refined by a riding model by placing them in calculated positions.

#### 3.3 Important structural parameters and refinement details

Crystal data and some of the important structural refinement parameters for sample **2** are given next. All of the details of the crystal data and structural refinement parameters are tabulated in Table S2.

**2(CCDC 2212626)**: C<sub>81</sub>H<sub>92</sub>Cl<sub>2</sub>Ni<sub>5</sub>S<sub>10</sub> ( $M_w = 1750.57$  g/mol): triclinic, space group P-1/m (no. 2),  $a = 16.3158(3)$  Å,  $b = 17.0494(3)$  Å,  $c = 17.7725(4)$  Å,  $\alpha = 61.5700(10)^\circ$ ,  $\beta = 70.3550(10)^\circ$ ,  $\gamma = 68.3270(10)^\circ$ ,  $V = 3961.73(14)$  Å<sup>3</sup>,  $Z = 2$ ,  $T = 100.15$  K,  $\mu(\text{MoK}\alpha) = 1.540$  mm<sup>-1</sup>,  $D_{\text{calc}} = 1.466$  g/cm<sup>3</sup>, 37,197 reflections measured ( $5.482^\circ \leq 2\theta \leq 50.748^\circ$ ), 13,420 unique ( $R_{\text{int}} = 0.0199$ ,  $R_{\text{sigma}} = 0.0223$ ) which were used in all calculations. The final  $R_1$  was 0.0331 [ $I > 2\sigma(I)$ ] and  $wR_2$  was 0.0756 (all data).

##### Refinement model description

Refinement model description

Number of restraints, 0; number of constraints, unknown.

##### Details:

###### 1. Fixed Uiso

At 1.2 times the following: all C(H) groups, all C(H,H) groups

###### 2. Others

Fixed Sof: C3(0.5) C1(0.5)

###### 3.a Secondary CH<sub>2</sub> refined with riding coordinates:

C00I(H00A,H00B), C00K(H00C,H00D), C00L(H00E,H00F), C00M(H00G,H00H), C00N(H00I,H00J), C00P(H00K,H00L), C00W(H00M,H00N), C00X(H00P,H00Q), C00Y(H00R,H00S), C00Z(H00U,H00V), C010(H01A,H01B), C012(H01C,H01D), C015(H01E,H01F), C019(H01G,

H01H), C01D(H01L,H01M), C01E(H01N,H01O), C01L(H01V,H01W), C01U(H4,H), C021(H02A,H02B), C02L(H02Q,H02R)

### 3.b Aromatic H refined with riding coordinates:

C00O(H00O), C00T(H00T), C013(H013), C014(H014), C02E(H02E), C02N(H02N), C02P(H02P), C02O(H02O), C02I(H02I), C018(H018), C01A(H01I), C01B(H01J), C01C(H01K), C01F(H01P), C01G(H01Q), C01H(H01R), C01I(H01S), C01J(H01T), C01K(H01U), C01M(H01X), C01O(H01Y), C01P(H01Z), C01Q(H01), C01R(H1), C01S(H2), C01T(H3), C01V(H5), C01W(H6), C01X(H7), C01Y(H8), C01Z(H9), C020(H020), C022(H022), C023(H023), C024(H024), C025(H025), C026(H026), C027(H027), C028(H028), C029(H029), C02A(H02C), C02B(H02D), C02C(H02F), C02D(H02G), C02F(H02H), C02G(H02J), C02H(H02K), C02J(H02L), C02K(H02M), C02M(H02S).

### 3.c Fitted hexagon refined as free rotating group:

C017 (C02E, C02N, C02P, C02O, C02I).

## 4. Electrochemical measurements

All electrochemical measurements for the oxygen evolution reaction (OER) were performed with an ECstat-302 (EC FRONTIER, Kyoto, Japan) with a RRDE-3A rotating ring disk electrode apparatus (BAS, Tokyo, Japan). A rotating disk electrode (RDE,  $\phi = 5$  mm) was polished with alumina paste and then sonicated in water before use. A Pt ring electrode was used as the counter electrode. A silver/silver chloride (Ag/AgCl) electrode was used as the reference electrode. In the setup, first the catalyst slurry was sonicated in an ice bath for 30 min, and then 10  $\mu$ L of the catalyst slurry was carefully dropped onto the RDE by the drop-cast method. After the catalyst slurry was sufficiently dried, each electrode was set in an electrochemical measurement system containing 0.10 mol L<sup>-1</sup> KOH (pH = 13) as the electrolyte (Fig. S2).

In the measurements, N<sub>2</sub> gas was bubbled for 30 min and then cyclic voltammetry (CV) was conducted 100 times in the region from 0 to 1.00 V (*vs.* reversible hydrogen electrode; RHE) at a scanning rate of 200 mV s<sup>-1</sup> for cleaning the electrodes.<sup>7</sup> After CV, linear sweep voltammetry (LSV) was performed under N<sub>2</sub> in the region from 1.0 to 1.75 V (*vs.* RHE) at a rate of 20 mV s<sup>-1</sup>. The measurements of LSV were also performed for the IrO<sub>x</sub>/CB catalyst and CB for a comparison purpose. The IrO<sub>x</sub>/CB catalyst was prepared using the method for the NiO-IM/CB catalysts with a slight modification. Specifically, CB (50 mg) was mixed with H<sub>2</sub>O (15 mL) and 2-propanol (15 mL), and the solution was sonicated for 10 min to disperse the CB in the mixture. Iridium tetrachloride (loading weight: 5 wt%) was added to the mixture, which was stirred at 140 °C for 1 h, resulting in volatilization of the solvent. The product was dried in a desiccator and subsequently calcined at 200 °C for 20 min, leading to the objective IrO<sub>x</sub>/CB.

In the durability test, LSV was performed 5 times in the region of 1.00–1.75 V (*vs.* RHE) at a scanning rate of 20 mV s<sup>-1</sup> with the RDE rotating at 1600 rpm. Chronopotentiometry (CP) was then performed for 1 h at a potential indicating 10 mA cm<sup>-2</sup> (1.96 mA) with the RDE rotating at 1600 rpm. This procedure was repeated four times for a total of 24 h to evaluate the stability.

## 5. Tables

**Table S1. Possible assignments of peaks observed in FT-IR spectra of Ni<sub>n</sub>(PET)<sub>2n</sub> (PET; phenylethane thiolate, *n* = 4, 5, 6)**

Wavenumber (cm <sup>-1</sup> )			Assignment <sup>a</sup>
Ni <sub>4</sub> (PET) <sub>8</sub>	Ni <sub>5</sub> (PET) <sub>10</sub>	Ni <sub>6</sub> (PET) <sub>12</sub>	
3059.5	3061.4	3061.4	ν(C-H) phenyl
3024.9	3025.8	3025.8	ν(C-H) phenyl
2956.3	2956.3	2957.3	ν(C-H) ethyl
2923.6	2923.6	2923.6	ν(C-H) ethyl
2852.3	2870.5	2870.5	ν(C-H) ethyl
1602.6	1603.5	1603.5	ν(C-C) phenyl
1495.5	1495.5	1495.5	ν(C-C) phenyl
1453.1	1453.1	1454.1	ν(C-C) phenyl or ethyl
1262.2	1264.1	1263.2	δ(C-H) phenyl or ethyl
1029.9	1029.9	1029.9	δ(C-H) phenyl
908.3	909.2	908.3	δ(C-H) phenyl
755.0	756.0	756.0	δ(C-H) phenyl
696.2	697.1	697.1	δ(C-H) phenyl

<sup>a</sup> See References<sup>8-11</sup>.

**Table S2. Crystal data and structure refinement for 2**

Identification code	<b>2</b>
Empirical formula	C <sub>81</sub> H <sub>92</sub> Cl <sub>2</sub> Ni <sub>5</sub> S <sub>10</sub>
Formula weight	1750.57
Temperature (K)	100.15
Crystal system	triclinic
Space group	P-1
a (Å)	16.3158(3)
b (Å)	17.0494(3)
c (Å)	17.7725(4)
α (°)	61.5700(10)
β (°)	70.3550(10)
γ (°)	68.3270(10)
Volume (Å <sup>3</sup> )	3961.73(14)
Z	2
ρ <sub>calc</sub> (g/cm <sup>3</sup> )	1.466
μ (mm <sup>-1</sup> )	1.540
F(000)	1820.0
Crystal size (mm <sup>3</sup> )	0.3 × 0.27 × 0.25
Radiation	MoKα (λ = 0.71073)
2θ range for data collection (°)	5.482 to 50.748
Index ranges	-19 ≤ h ≤ 19, -20 ≤ k ≤ 15, -21 ≤ l ≤ 21
Reflections collected	37,197
Independent reflections	13,420 [R <sub>int</sub> = 0.0199, R <sub>sigma</sub> = 0.0223]
Data/restraints/parameters	13420/0/880
Goodness-of-fit on F <sup>2</sup>	1.019
Final R indexes [I >= 2σ (I)]	R <sub>1</sub> = 0.0331, wR <sub>2</sub> = 0.0726
Final R indexes [all data]	R <sub>1</sub> = 0.0370, wR <sub>2</sub> = 0.0756
Largest diff. peak/hole (e Å <sup>-3</sup> )	1.88/-2.05

**Table S3. Molecular distances for Ni<sub>n</sub>(PET)<sub>2n</sub> (n = 4, 5, 6)**

Sample	Ni-S (Å)	Ni-Ni (Å)	Ni-center of gravity (Å)
Ni <sub>4</sub> (PET) <sub>8</sub>	2.211 ± 0.0057	2.672 ± 0.0130	1.889 ± 0.0111
Ni <sub>5</sub> (PET) <sub>10</sub>	2.204 ± 0.0114	2.816 ± 0.0714	2.393 ± 0.1160
Ni <sub>6</sub> (PET) <sub>12</sub>	2.199 ± 0.0123	2.928 ± 0.0615	2.924 ± 0.1460

**Table S4. Molecular angles for Ni<sub>n</sub>(PET)<sub>2n</sub> (n = 4, 5, 6)**

Sample	Ni-S-Ni (°)	S-Ni-S (°)	Ni-Ni-Ni (°)
Ni <sub>4</sub> (PET) <sub>8</sub>	74.3 ± 0.47	97.6 ± 0.37	90.0 ± 0.67
Ni <sub>5</sub> (PET) <sub>10</sub>	79.4 ± 2.60	98.3 ± 4.60	108.0 ± 5.92
Ni <sub>6</sub> (PET) <sub>12</sub>	83.5 ± 2.20	98.1 ± 1.20	120.0 ± 5.88

**Table S5. Molecular distances for Ni<sub>5</sub>(SR)<sub>10</sub> (SR = thiolate)**

Sample	Ni-S (Å)	Ni-Ni (Å)	Ni-center of gravity (Å)
Ni <sub>5</sub> (PET) <sub>10</sub>	2.204 ± 0.0114	2.816 ± 0.0714	2.393 ± 0.1160
Ni <sub>5</sub> (SCH <sub>2</sub> SiMe <sub>3</sub> ) <sub>10</sub>	2.216 ± 0.0095	2.835 ± 0.0187	2.410 ± 0.0409
Ni <sub>5</sub> (SCH <sub>2</sub> CH <sub>3</sub> ) <sub>10</sub>	2.199 ± 0.0125	2.816 ± 0.0631	2.393 ± 0.0872

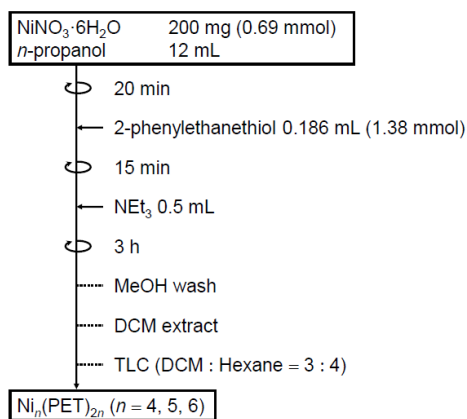
**Table S6. Molecular angles for Ni<sub>n</sub>(SR)<sub>2n</sub> (n = 4, 5, 6)**

Sample	Ni-S-Ni (°)	S-Ni-S (°)	Ni-Ni-Ni (°)
Ni <sub>5</sub> (PET) <sub>10</sub>	79.4 ± 2.60	98.3 ± 4.60	108.0 ± 5.92
Ni <sub>5</sub> (SCH <sub>2</sub> SiMe <sub>3</sub> ) <sub>10</sub>	79.5 ± 0.66	98.2 ± 4.57	108.0 ± 2.15
Ni <sub>5</sub> (SCH <sub>2</sub> CH <sub>3</sub> ) <sub>10</sub>	79.6 ± 2.25	98.3 ± 4.44	108.4 ± 4.86

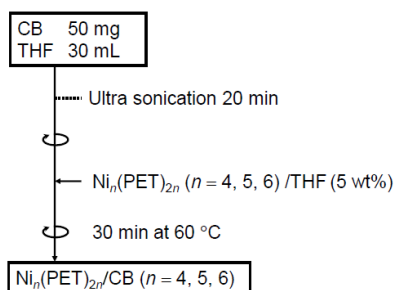
**Table S7. OER activity for Ni<sub>n</sub>(PET)<sub>2n</sub>/CB (n = 4, 5, 6) and NiO-IM/CB**

Sample	Over-potential at 10 mA cm <sup>-2</sup> (V)	OER mass activity at 1.55 V vs. RHE (A mg <sub>Ni</sub> <sup>-1</sup> )	Tafel slope (mV dec <sup>-1</sup> )
Ni <sub>4</sub> (PET) <sub>8</sub> /CB	359	3.65	58.5
Ni <sub>5</sub> (PET) <sub>10</sub> /CB	345	5.65	57.2
Ni <sub>6</sub> (PET) <sub>12</sub> /CB	360	3.70	54.8
NiO-IM/CB	376	2.50	64.5

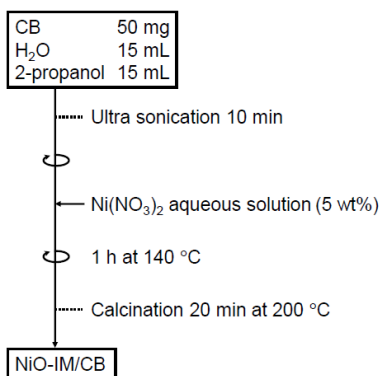
## 6. Additional schemes



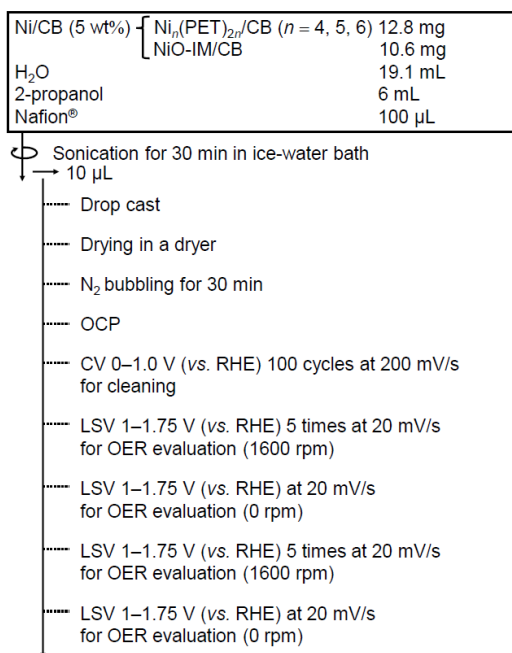
**Scheme S1** Synthesis protocol used for  $\text{Ni}_n(\text{PET})_{2n}$  ( $n = 4, 5, 6$ ).



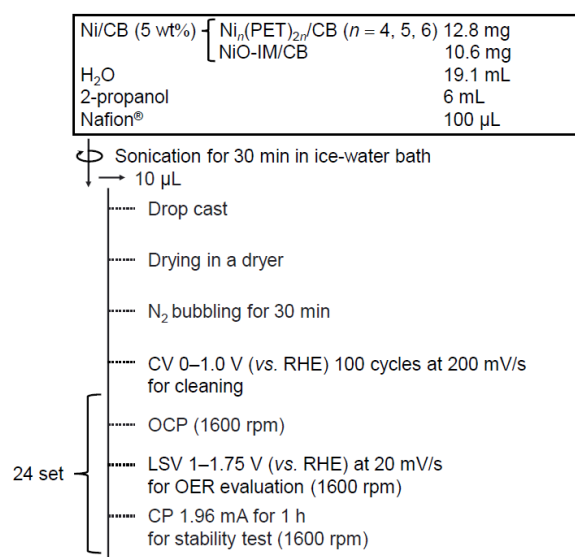
**Scheme S2** Preparation protocol used for  $\text{Ni}_n(\text{PET})_{2n}/\text{CB}$  ( $n = 4, 5, 6$ ).



**Scheme S3** Preparation protocol used for NiO-IM/CB (IM; impregnation).



**Scheme S4** Protocol used for electrochemical measurements.



**Scheme S5** Protocol used for stability experiment.

## 7. Additional figures

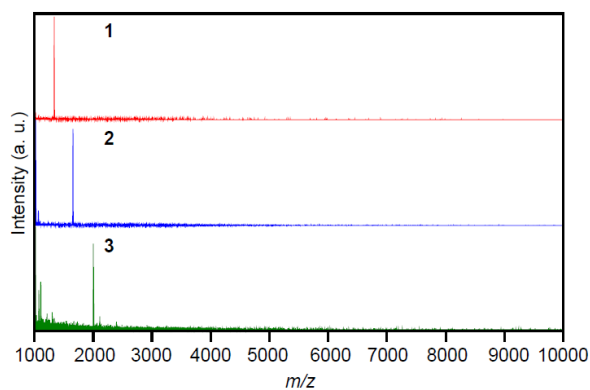


**Fig. S1** Positive-ion MALDI mass spectra of synthesized  $[\text{Ni}_4(\text{PET})_8]^0$  (**1**),  $[\text{Ni}_5(\text{PET})_{10}]^0$  (**2**), and  $[\text{Ni}_6(\text{PET})_{12}]^0$  (**3**) with wide  $m/z$  range.

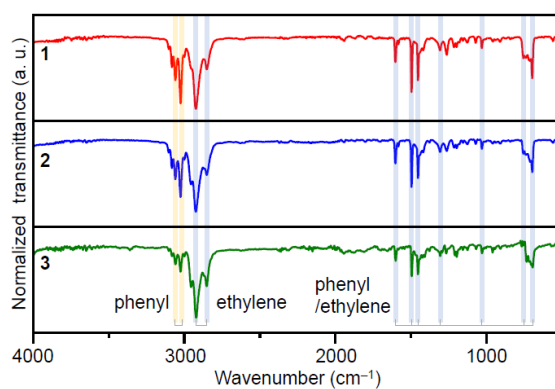


**Fig. S2** FT-IR spectra of synthesized **1–3**. Absorption at ca. 3000 and 800–1500  $\text{cm}^{-1}$  indicate that PET are included as a ligand in **1–3**.<sup>8–11</sup>

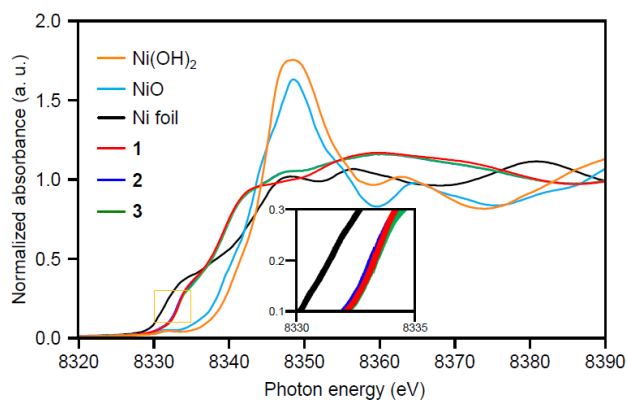


**Fig. S3** Results of Ni K-edge XANES spectra for synthesized **1–3** together with Ni foil, NiO, and Ni(OH)<sub>2</sub>. Inset shows the enlarged spectra.

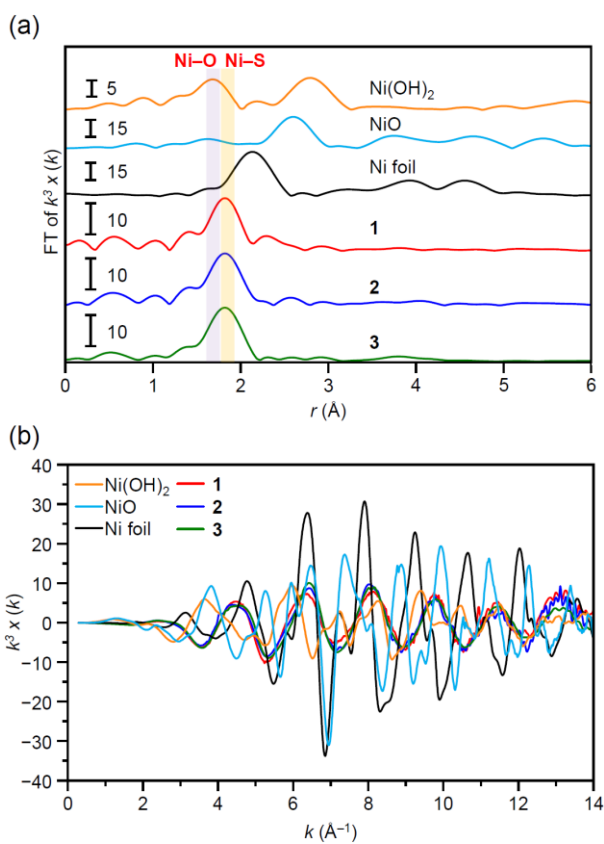


**Fig. S4** Results of Ni K-edge (a) FT-EXAFS and (b) EXAFS spectra for synthesized **1–3** together with Ni foil, NiO, and Ni(OH)<sub>2</sub>. In (a), the peaks at 1.7 and 1.8 Å are assigned to the Ni–O and Ni–S bond, respectively<sup>12–16</sup>.

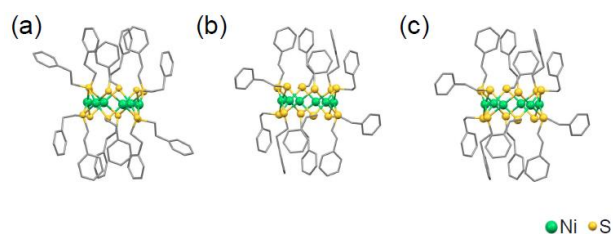


**Fig. S5** Geometric structures for (a) [Ni<sub>6</sub>(PET)<sub>12</sub>]<sup>0</sup> determined by SC-XRD from Ref. 17 (3) and calculated for [Ni<sub>6</sub>(PET)<sub>12</sub>]<sup>0</sup> in (b) THF solution (3') and (c) vacuum (3'').

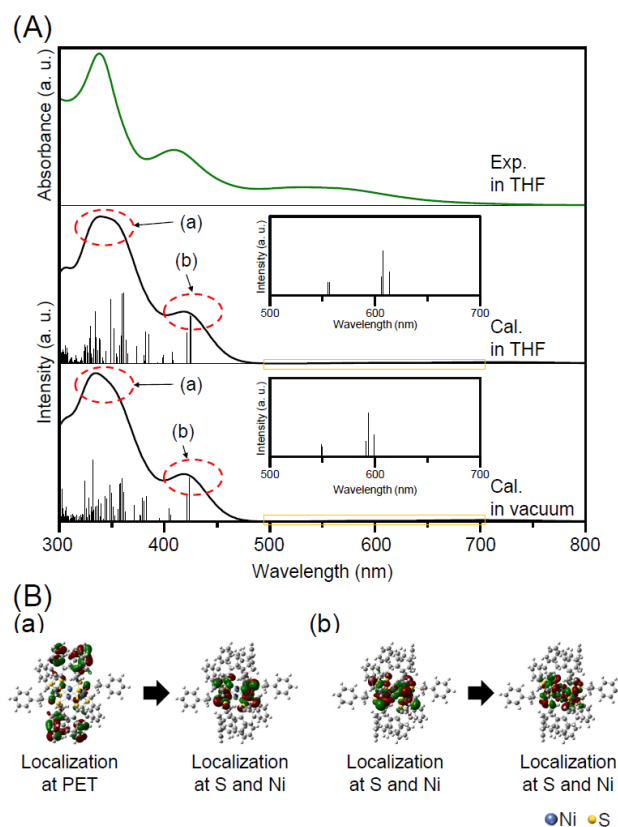


**Fig. S6** (A) (top) Optical absorption spectrum of [Ni<sub>6</sub>(PET)<sub>12</sub>]<sup>0</sup> in THF and calculated absorption spectra of [Ni<sub>6</sub>(PET)<sub>12</sub>]<sup>0</sup> (middle) in THF and (bottom) in vacuum. (B) Molecular orbitals of the transition at (a) (Aa) and (b) (Ab) for [Ni<sub>6</sub>(PET)<sub>12</sub>]<sup>0</sup>. Ni: light blue, S: yellow, carbon: dark gray, and hydrogen: light gray.

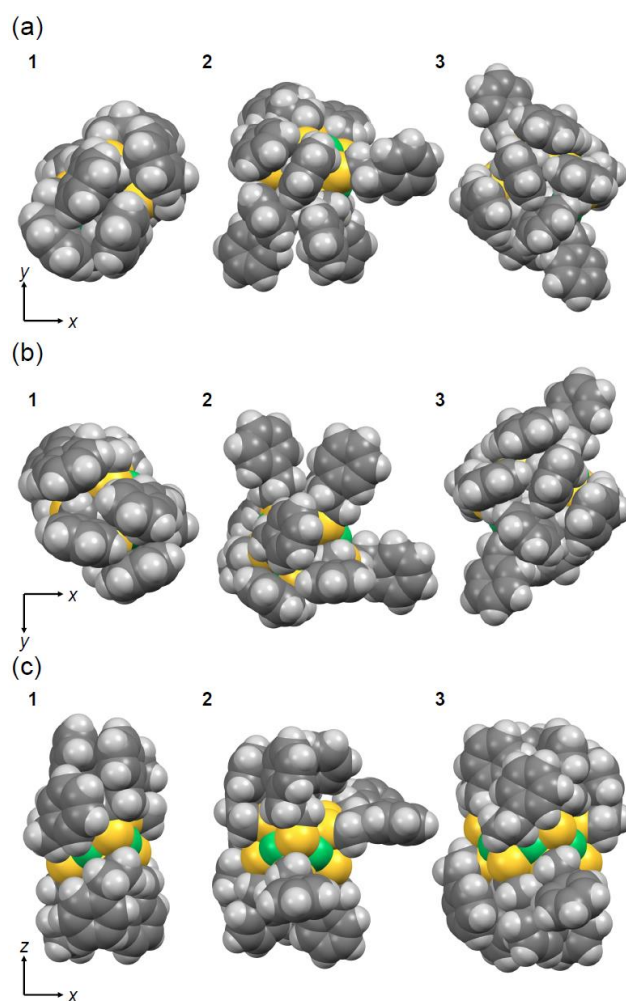


**Fig. S7** Space-filling models of (left) **1**, (middle) **2**, and (right) **3** from (a) top, (b) bottom, and (c) side views. The geometric structure of **1**, and **3** were obtained from Ref. 17. Ni: light green, S: yellow, dark gray: carbon, and light gray: hydrogen.

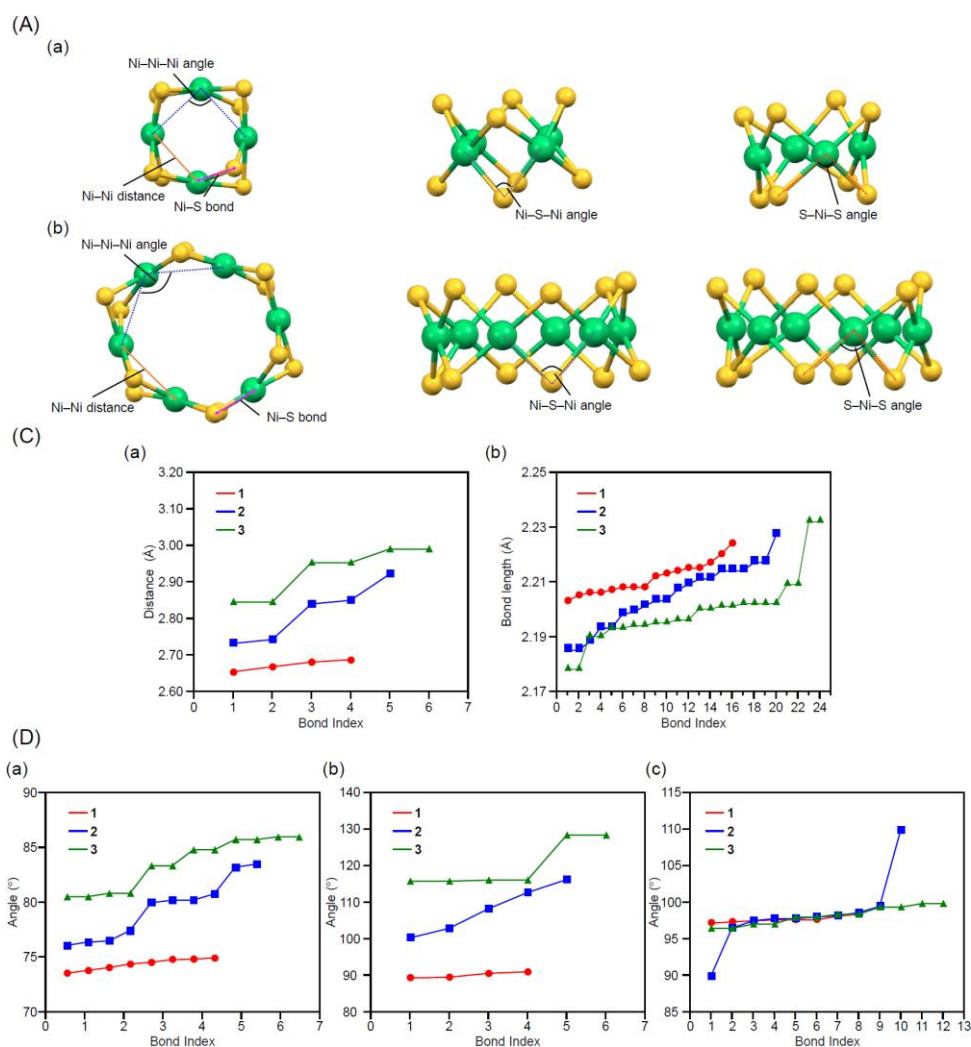


**Fig. S8** (A) The relevant geometric parameters of the structure for (a) **1** and (b) **3**. (B) Bond length [(a) Ni-Ni distance and (b) Ni-S bond], and (C) bond angles [(a) Ni-S-Ni, (b) Ni-Ni-Ni and (c) S-Ni-S angles] from the analysis of geometric structures for **1-3** determined by SC-XRD. For **1** and **3**, the parameter estimated by the crystal structure from Ref. 17.

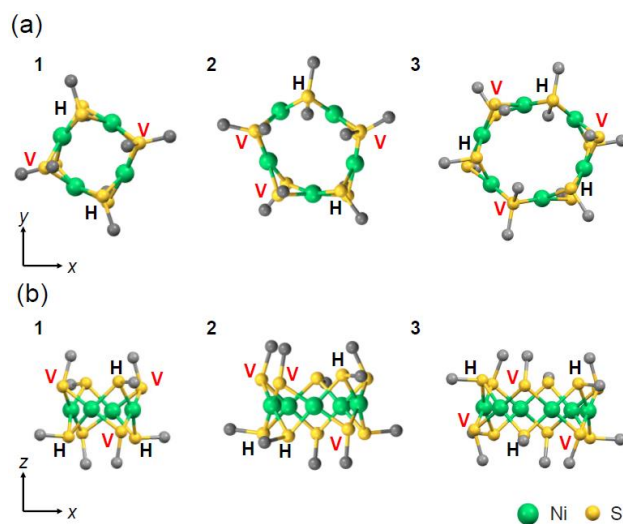


**Fig. S9** Geometric structures for (left) **1**, (middle) **2**, and (right) **3** from (a) top and (b) side views. V and H indicate the S sites connected with vertical (V site) and horizontal (H site) carbon chain, respectively. Although **1** and **3** have alternately arranged PET ligands because of the even number of S atoms, PET ligands with complete alternating placement in **2** are prohibited because of the odd number of SR ligands. The geometric structure of **1**, and **3** were obtained from Ref. 17.

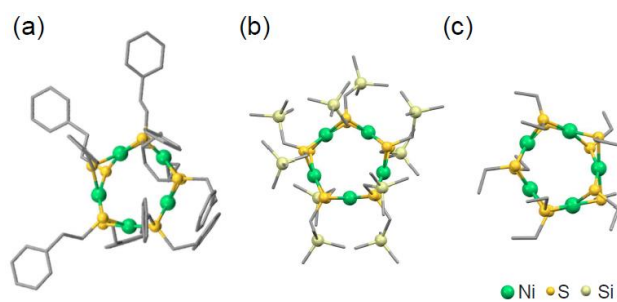


**Fig. S10** Geometrical structures for (a)  $[\text{Ni}_5(\text{PET})_{10}]^0$ , (b)  $[\text{Ni}_5(\text{SCH}_2\text{SiMe}_3)_{10}]^0$ , and (c)  $[\text{Ni}_5(\text{SCH}_2\text{CH}_3)_{10}]^0$ . The geometric structure of  $[\text{Ni}_5(\text{SCH}_2\text{SiMe}_3)_{10}]^0$ , and  $[\text{Ni}_5(\text{SCH}_2\text{CH}_3)_{10}]^0$  were obtained from Ref. 18 and 19.

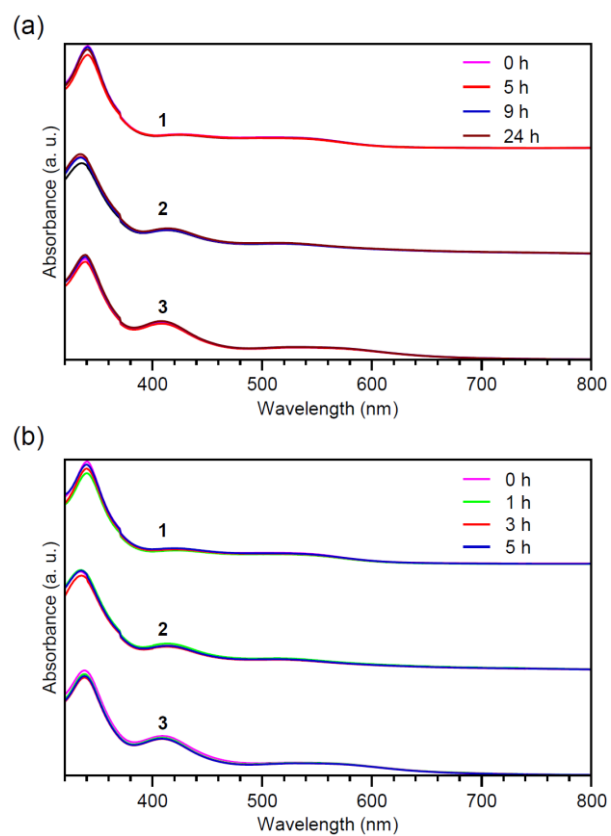


**Fig. S11** Time dependence of the changes in the optical absorption spectra of (top) **1**, (middle) **2**, and (bottom) **3** in THF at (a) 25 °C and (b) 60 °C.

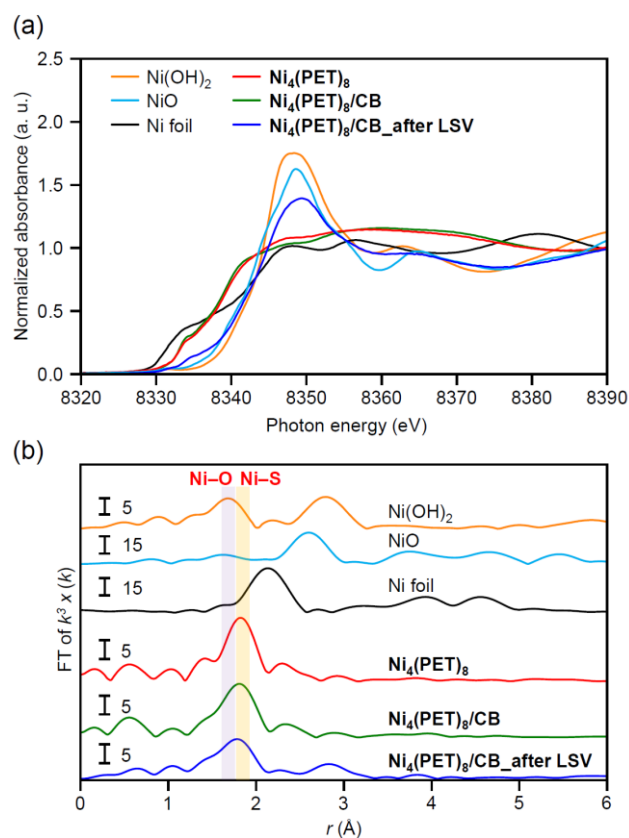


**Fig. S12** Results of Ni K-edge (a) XANES and (b) FT-EXAFS spectra for  $[\text{Ni}_4(\text{PET})_8]^0$ ,  $\text{Ni}_4(\text{PET})_8/\text{CB}$ , and  $\text{Ni}_4(\text{PET})_8/\text{CB}$  after LSV together with Ni foil, NiO, and  $\text{Ni}(\text{OH})_2$ . There was no substantial changes in the geometric/electronic structures of  $\text{Ni}_4(\text{PET})_8$  before and after adsorption of **1** on CB.

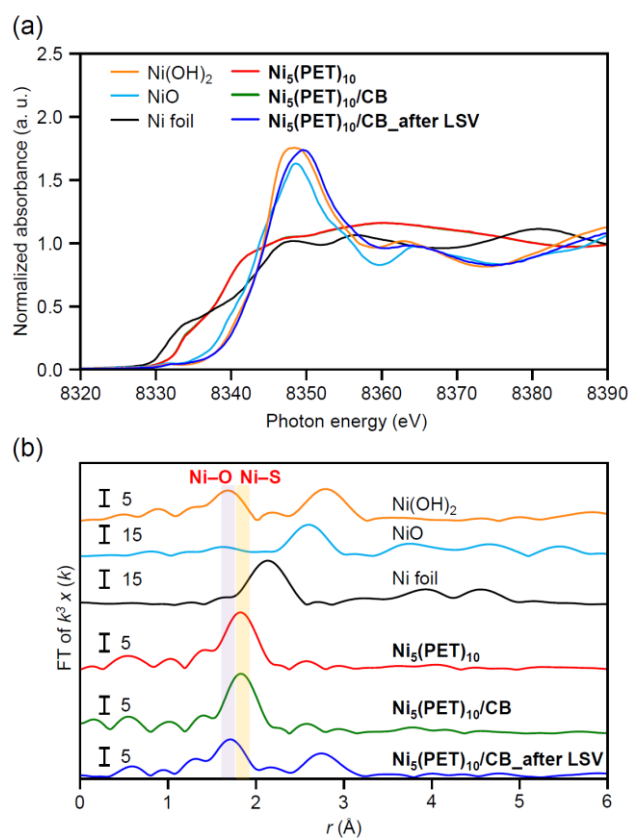


**Fig. S13** Results of Ni K-edge (a) XANES and (b) FT-EXAFS spectra for  $[\text{Ni}_5(\text{PET})_{10}]^0$ ,  $\text{Ni}_5(\text{PET})_{10}/\text{CB}$ , and  $\text{Ni}_5(\text{PET})_{10}/\text{CB}$  after LSV together with Ni foil, NiO, and  $\text{Ni}(\text{OH})_2$ . There was no substantial change in the geometric/electronic structures of  $\text{Ni}_5(\text{PET})_{10}$  before and after adsorption of **2** on CB.

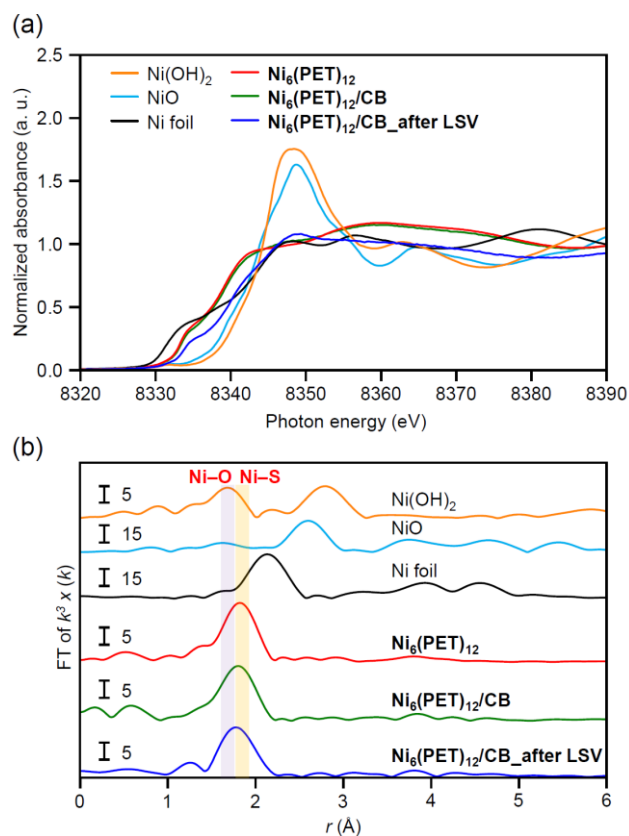


**Fig. S14** Results of Ni K-edge (a) XANES and (b) FT-EXAFS spectra for  $[\text{Ni}_6(\text{PET})_{12}]^0$ ,  $\text{Ni}_6(\text{PET})_{12}/\text{CB}$ , and  $\text{Ni}_6(\text{PET})_{12}/\text{CB}$  after LSV together with Ni foil, NiO, and  $\text{Ni}(\text{OH})_2$ . There was no substantial change in the geometric/electronic structures of  $\text{Ni}_6(\text{PET})_{12}$  before and after adsorption of **3** on CB.

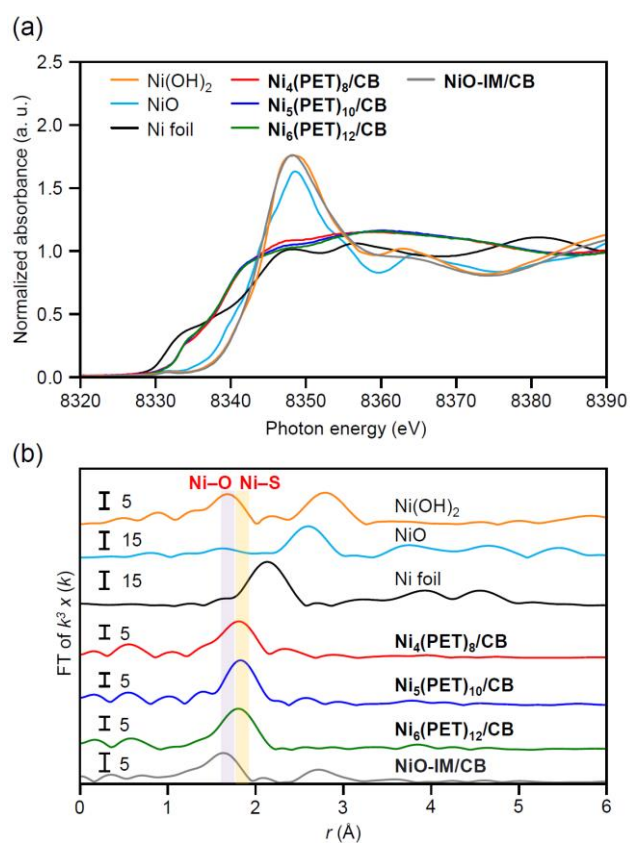


**Fig. S15** Results of Ni K-edge (a) XANES and (b) FT-EXAFS spectra for Ni<sub>*n*</sub>(PET)<sub>2*n*</sub>/CB (*n* = 4, 5, 6) together with Ni foil, NiO, and Ni(OH)<sub>2</sub>.

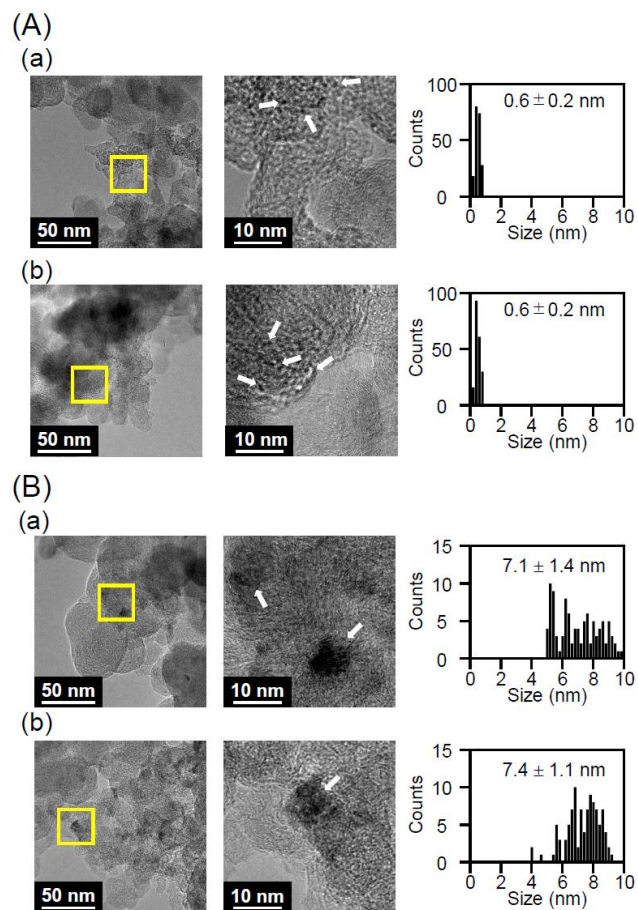


**Fig. S16** (left and middle) TEM images and (right) resulting histograms of particle-size distribution of (A)  $\text{Ni}_5(\text{PET})_{10}/\text{CB}$  and (B)  $\text{NiO-IM}/\text{CB}$  (a) before and (b) after electrochemical measurements. In (a) and (b), loading weight of Ni on CB is 5 wt%.

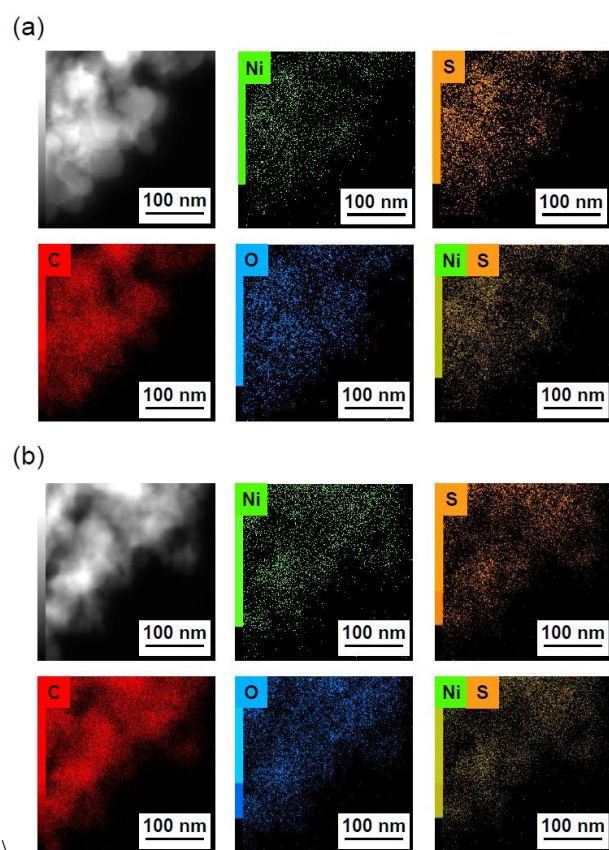


**Fig. S17** HAADF-STEM images and EDS elemental mapping (Ni, S, C, and O) of Ni<sub>5</sub>(PET)<sub>10</sub>/CB (a) before and (b) after electrochemical measurements. In (a) and (b), loading weight of Ni on CB is 5 wt%.

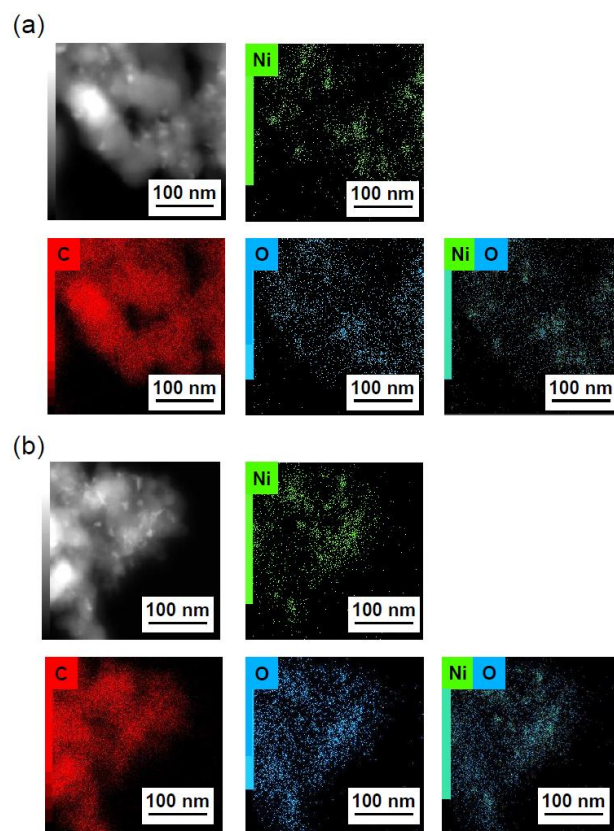


**Fig. S18** HAADF-STEM images and EDS elemental mapping (Ni, C, and O) of NiO-IM/CB (a) before and (b) after electrochemical measurements. In (a) and (b), loading weight of Ni on CB is 5 wt%.

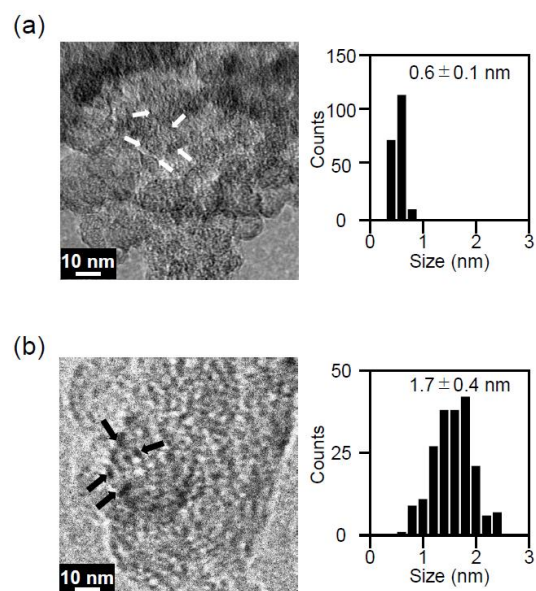


**Fig. S19** (left) TEM images and (right) resulting histograms of particle-size distribution of (a)  $\text{Ni}_5(\text{PET})_{10}/\text{CB}$  and (b)  $\text{NiO-IM}/\text{CB}$ . In (a) and (b), loading weight of Ni on CB is 0.5 wt%.

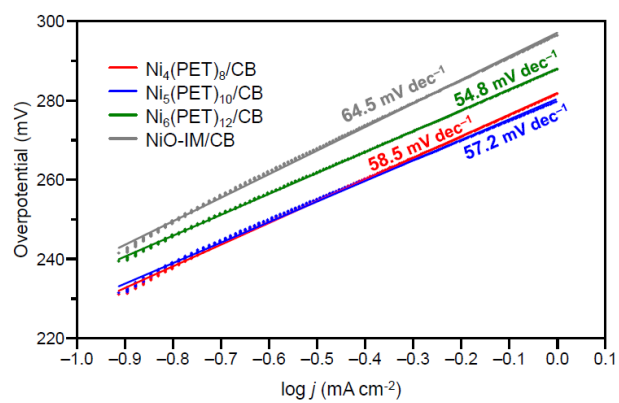


**Fig. S20** Tafel slope of for  $\text{Ni}_n(\text{PET})_{2n}/\text{CB}$  ( $n = 4, 5, 6$ ) and  $\text{NiO-IM/CB}$  on a GC electrode in 0.1 M KOH. Ni loading weight of all samples is 5 wt%.

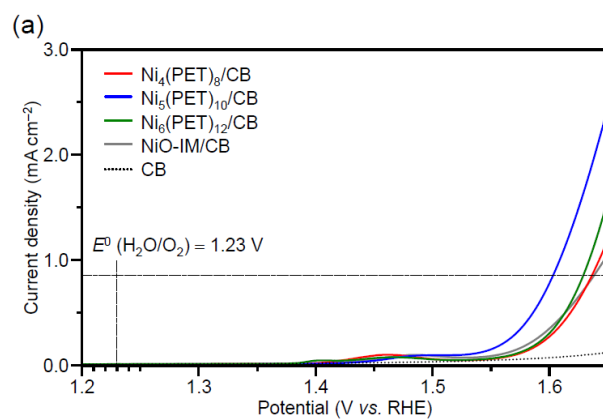


**Fig. S21** LSV curves for  $\text{Ni}_n(\text{PET})_{2n}/\text{CB}$  ( $n = 4, 5, 6$ ) and  $\text{NiO-IM}/\text{CB}$  on a GC electrode in 0.1 M KOH. Ni loading weight of all samples is 0.5 wt%.

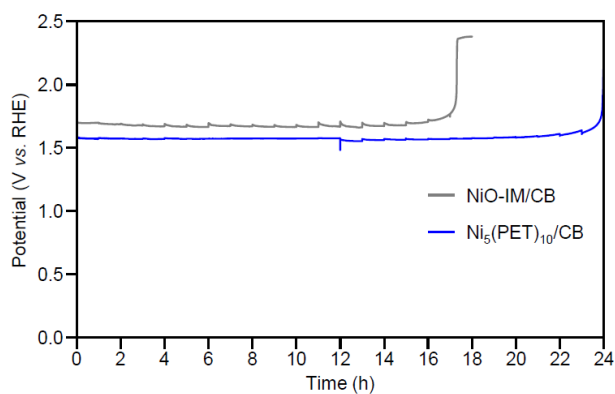


**Fig. S22** Chronopotentiometry curves for Ni<sub>5</sub>(PET)<sub>10</sub>/CB and NiO-IM/CB collected at 10 mA cm<sup>-2</sup> for 24 hours on GC electrodes in 0.1 M KOH. Ni loading weight of all samples was set to 5 wt%. The significant incensement of overpotential after 17 hours and 24 hours for NiO-IM/CB and Ni<sub>5</sub>(PET)<sub>10</sub>/CB, respectively, is due to the dropping out of the catalysts from electrodes by oxygen evolution for long time measurements.

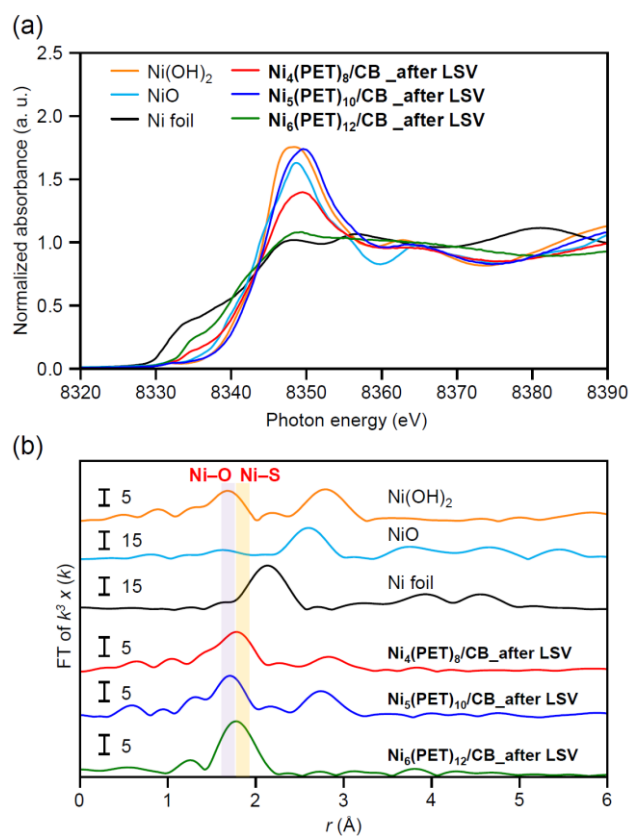


**Fig. S23** Results of Ni K-edge (a) XANES and (b) FT-EXAFS spectra for Ni<sub>*n*</sub>(PET)<sub>2*n*</sub>/CB (*n* = 4, 5, 6) after LSV together with Ni foil, NiO, and Ni(OH)<sub>2</sub>.

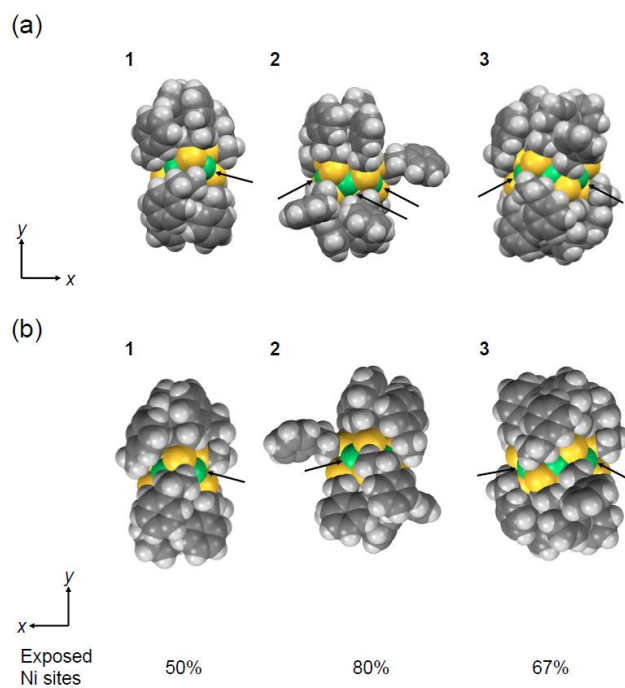


**Fig. S24** Space-filling models of (left) **1**, (middle) **2**, and (right) **3** from (a) front and (b) back views. In (ab), arrows indicate exposed Ni sites. The geometric structure of **1**, and **3** were obtained from Ref. 17. Ni: light green, S: yellow, dark gray: carbon, and light gray: hydrogen.

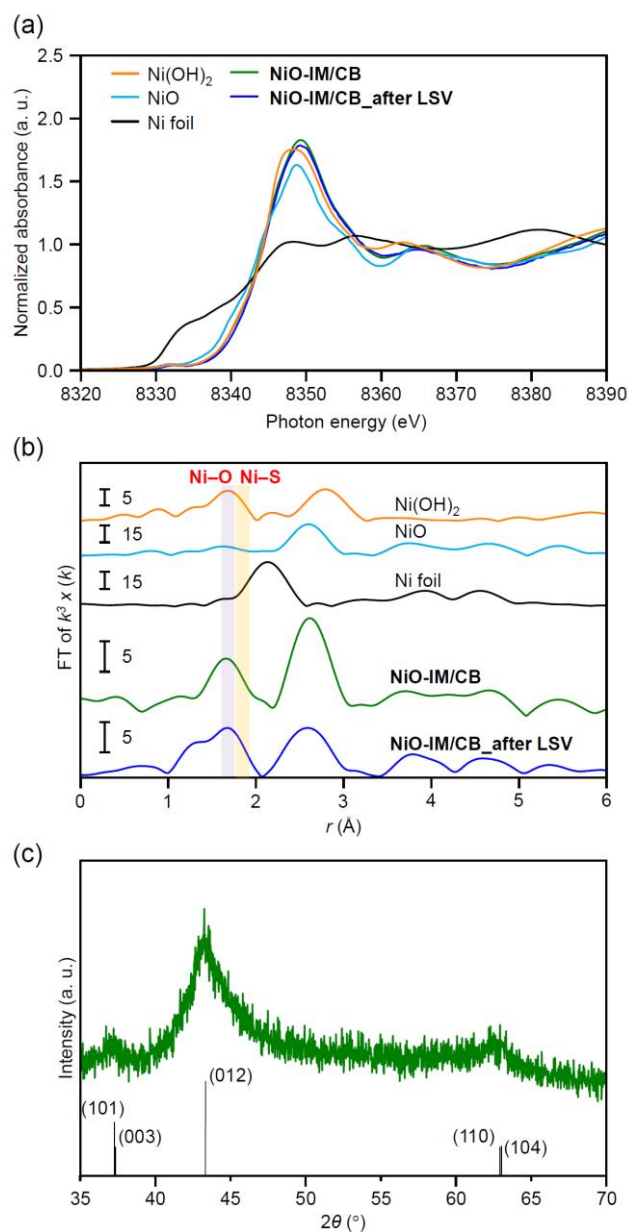


**Fig. S25** Results of Ni K-edge (a) XANES and (b) FT-EXAFS spectra for NiO-IM/CB before and after LSV together with Ni foil, NiO, and Ni(OH)<sub>2</sub>. (c) PXRD patterns for NiO-IM/CB before LSV.

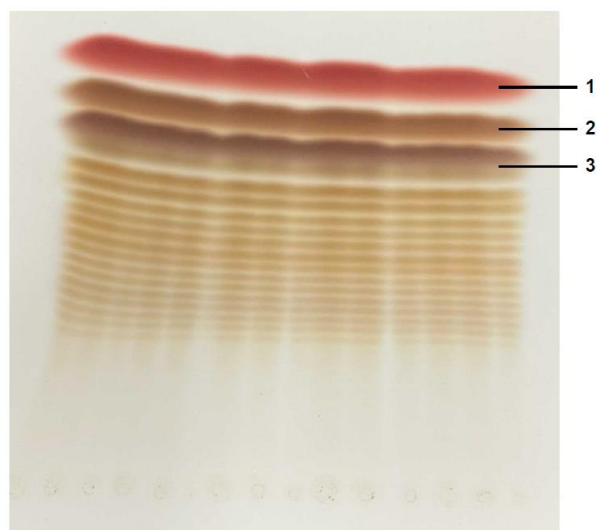


**Fig. S26** Photograph of the plate for thin layer chromatography after separation of the synthesized products.

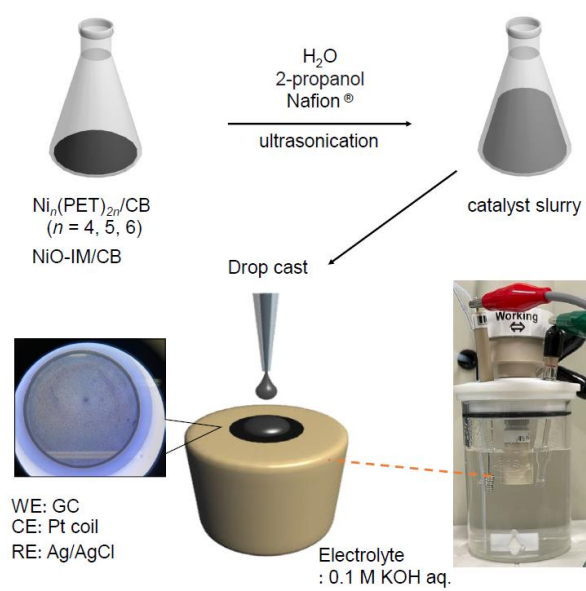


**Fig. S27.** Schematic of the setup for electrochemical experiments.

## 6. References

- [1] H. Asakura, S. Yamazoe, T. Misumi, A. Fujita, T. Tsukuda and T. Tanaka, *Radiat. Phys. Chem.*, 2020, **175**, 108270.
- [2] M. J. Frisch, G. W. Trucks, H. B. Schlegel, G. E. Scuseria, M. A. Robb, J. R. Cheeseman, G. Scalmani, V. Barone, G. A. Petersson, H. Nakatsuji, X. Li, M. Caricato, A. V. Marenich, J. Bloino, B. G. Janesko, R. Gomperts, B. Mennucci, H. P. Hratchian, J. V. Ortiz, A. F. Izmaylov, J. L. Sonnenberg, D. Williams-Young, F. Ding, F. Lipparini, F. Egidi, J. Goings, B. Peng, A. Petrone, T. Henderson, D. Ranasinghe, V. G. Zakrzewski, J. Gao, N. Rega, G. Zheng, W. Liang, M. Hada, M. Ehara, K. Toyota, R. Fukuda, J. Hasegawa, M. Ishida, T. Nakajima, Y. Honda, O. Kitao, H. Nakai, T. Vreven, K. Throssell, J. A. Montgomery, Jr., J. E. Peralta, F. Ogliaro, M. J. Bearpark, J. J. Heyd, E. N. Brothers, K. N. Kudin, V. N. Staroverov, T. A. Keith, R. Kobayashi, J. Normand, K. Raghavachari, A. P. Rendell, J. C. Burant, S. S. Iyengar, J. Tomasi, M. Cossi, J. M. Millam, M. Klene, C. Adamo, R. Cammi, J. W. Ochterski, R. L. Martin, K. Morokuma, O. Farkas, J. B. Foresman, and D. J. Fox, GAUSSIAN 16 (Revision A.03), Gaussian, Inc., Wallingford, CT, 2016.
- [3] G. M. Sheldrick, *Acta Crystallogr., Sect. A: Found. Adv.*, 2015, **71**, 3–8.
- [4] Bruker APEX4 (v2021.10–0), Bruker AXS Inc., Madison, WI, USA, 2021.
- [5] G. M. Sheldrick, *Acta Crystallogr., Sect. C: Struct. Chem.*, 2015, **71**, 3–8.
- [6] O. V. Dolomanov, L. J. Bourhis, R. J. Gildea, J. A. K. Howard and H. Puschmann, *J. Appl. Crystallogr.*, 2009, **42**, 339–341.
- [7] C. Wei, R. R. Rao, J. Peng, B. Huang, I. E. L. Stephens, M. Risch, Z. J. Xu and Y. Shao-Horn, *Adv. Mater.*, 2019, **31**, 1806296.
- [8] H. G. M. Edwards, A. F. Johnson and I. R. Lewis, *Spectrochim. Acta, Part A*, 1993, **49**, 707–714.
- [9] L. V. Nair, S. Hossain, S. Wakayama, S. Takagi, M. Yoshioka, J. Maekawa, A. Harasawa, B. Kumar, Y. Niihori, W. Kurashige and Y. Negishi, *J. Phys. Chem. C*, 2017, **121**, 11002–11009.
- [10] J. Ji, G. Wang, T. Wang, X. You and X. Xu, *Nanoscale*, 2014, **6**, 9185–9191.
- [11] A. M. S. Pembere, C. Cui, R. Anumula, H. Wu, P. An, T. Liang and Z. Luo, *Phys. Chem. Chem. Phys.*, 2019, **21**, 17933–17938.
- [12] Q. Li, D. Wang, C. Han, X. Ma, Q. Lu, Z. Xing and X. Yang, *J. Mater. Chem. A*, 2018, **6**, 8233–8237.
- [13] Y. Hattori, T. Konishi and K. Kaneko, *Chem. Phys. Lett.*, 2002, **355**, 37–42.
- [14] Q. Ma, C. Hu, K. Liu, S.-F. Hung, D. Ou, H. M. Chen, G. Fu and N. Zheng, *Nano Energy*, 2017, **41**, 148–153.
- [15] M. A. Peck and M. A. Langell, *Chem. Mater.*, 2012, **24**, 4483–4490.
- [16] G. Zhao, P. Li, N. Cheng, S. X. Dou and W. Sun, *Adv. Mater.*, 2020, **32**, 2000872.
- [17] K. S. Joya, L. Sinatra, L. G. AbdulHalim, C. P. Joshi, M. N. Hedhili, O. M. Bakr and I. Hussain, *Nanoscale*, 2016, **8**, 9695–9703.
- [18] B.-K. Koo, E. Block, H. Kang, S. Liu and J. Zubieta, *Polyhedron*, 1988, **7**, 1397–1399.
- [19] M. Kriege and G. Henkel, *Z. Naturforsch. B*, 1987, **42**, 1121–1128.